



Article

High-Throughput Phenotyping: Application in Maize Breeding

Ewerton Lélys Resende ^{1,*} , Adriano Teodoro Bruzi ^{2,*}, Everton da Silva Cardoso ¹, Vinícius Quintão Carneiro ¹, Vitório Antônio Pereira de Souza ¹, Paulo Henrique Frois Correa Barros ² and Raphael Rodrigues Pereira ²

¹ Departamento de Biologia, Universidade Federal de Lavras, Lavras 37203-202, MG, Brazil; cardoso.xs@hotmail.com (E.d.S.C.); vinicius.carneiro@ufla.br (V.Q.C.); vitorioapsoza@gmail.com (V.A.P.d.S.)

² Departamento de Agricultura, Universidade Federal de Lavras, Lavras 37203-202, MG, Brazil; paulo.barros@estudante.ufla.br (P.H.F.C.B.); raphael.pereira1@estudante.ufla.br (R.R.P.)

* Correspondence: elresendeagro@outlook.com (E.L.R.); adrianobruzi@ufla.br (A.T.B.)

Abstract: In breeding programs, the demand for high-throughput phenotyping is substantial as it serves as a crucial tool for enhancing technological sophistication and efficiency. This advanced approach to phenotyping enables the rapid and precise measurement of complex traits. Therefore, the objective of this study was to estimate the correlation between vegetation indices (VIs) and grain yield and to identify the optimal timing for accurately estimating yield. Furthermore, this study aims to employ photographic quantification to measure the characteristics of corn ears and establish their correlation with corn grain yield. Ten corn hybrids were evaluated in a Complete Randomized Block (CRB) design with three replications across three locations. Vegetation and green leaf area indices were estimated throughout the growing cycle using an unmanned aerial vehicle (UAV) and were subsequently correlated with grain yield. The experiments consistently exhibited high levels of experimental quality across different locations, characterized by both high accuracy and low coefficients of variation. The experimental quality was consistently significant across all sites, with accuracy ranging from 79.07% to 95.94%. UAV flights conducted at the beginning of the crop cycle revealed a positive correlation between grain yield and the evaluated vegetation indices. However, a positive correlation with yield was observed at the V5 vegetative growth stage in Lavras and Ijaci, as well as at the V8 stage in Nazareno. In terms of corn ear phenotyping, the regression coefficients for ear width, length, and total number of grains (TNG) were 0.92, 0.88, and 0.62, respectively, demonstrating a strong association with manual measurements. The use of imaging for ear phenotyping is promising as a method for measuring corn components. It also enables the identification of the optimal timing to accurately estimate corn grain yield, leading to advancements in the agricultural imaging sector by streamlining the process of estimating corn production.

Keywords: crop genetics; biometrics; data acquisition and assimilation



Citation: Resende, E.L.; Bruzi, A.T.; Cardoso, E.d.S.; Carneiro, V.Q.; Pereira de Souza, V.A.; Frois Correa Barros, P.H.; Pereira, R.R. High-Throughput Phenotyping: Application in Maize Breeding. *AgriEngineering* **2024**, *6*, 1078–1092. <https://doi.org/10.3390/agriengineering6020062>

Academic Editors: Giovanni Rallo, Changyuan Zhai, Ning Wang and Jianfeng Zhou

Received: 11 December 2023

Revised: 14 February 2024

Accepted: 5 March 2024

Published: 20 April 2024



Copyright: © 2024 by the authors. Licensee MDPI, Basel, Switzerland. This article is an open access article distributed under the terms and conditions of the Creative Commons Attribution (CC BY) license (<https://creativecommons.org/licenses/by/4.0/>).

1. Introduction

The demand for high-throughput phenotyping has become increasingly critical across agricultural and plant breeding sectors and the seed industry. As a key driver of technological advancement and operational efficiency, this sophisticated method of phenotyping facilitates the rapid and accurate assessment of complex traits. The resultant acceleration in the selection process not only improves breeding programs but also substantially boosts genetic improvement in crop varieties. Additionally, it is mainly driven by the need to understand genotype-by-environment interactions [1]. Thus, improving traits of interest depends on the ability to quantify phenotypes across genotypes replicated over multiple environments [2]. Traditionally, field phenotypic data have been obtained manually, a labor-intensive and time-consuming process that limits the number of measurable traits [3]. However, the expansion of technologies has enabled cost-effective high-throughput phenotyping (HTP) to automatically acquire multisource crop data, which can greatly reduce the manual labor and time required to obtain crop phenotypic information [4].

With HTP, our understanding of crop development is enhanced, bridging the gaps in the relationship between genotype and phenotype [5]. Numerous phenotyping platforms are available to achieve this goal, with aerial phenotyping in the field being a preferred approach. Aerial phenotyping primarily leverages unmanned aerial vehicles (UAVs) equipped with a variety of sensors, including visible-light (RGB) cameras, infrared thermal imagers, LiDAR, multispectral cameras, and hyperspectral sensors. An essential criterion for these sensors is cost-effectiveness, with RGB cameras being a prime example [6]. For instance, studies have employed RGB cameras to predict rice (*Oryza sativa*) yield, and similar cameras have been used to estimate yield and other traits in crops such as wheat (*Triticum* spp.), soybean (*Glycine max*), maize (*Zea mays*), barley (*Hordeum vulgare*), and potatoes (*Solanum tuberosum*) [7–12].

After acquiring images through these technologies, a range of traits related to growth, development, tolerance, resistance, architecture, physiology, ecology, and yield can be estimated. In particular, many studies have employed digital images to derive vegetation indices (VIs), which are powerful tools for assessing green vegetation. [7] demonstrated the effectiveness of color indices, such as the Excess Green (ExG) and Visible Atmospherically Resistant Index (VARI) calculated from RGB images, in mapping vegetation fractions and their high correlations with rice grain yield. The Normalized Green-Red Difference Index (NGRDI), derived from RGB images, also exhibited strong correlations with the aboveground biomass of peas and oats, with R^2 values ranging from 0.58 to 0.78 [13].

In the context of corn crops, the correlation between VIs and yield varies based on the growth stage and the specific index used, with VARI being one of the top-performing indices. Additionally, canopy cover at 47 and 79 days after sowing has shown a strong correlation with corn yield in some populations, with correlations to grain yield of 0.76 and 0.77, respectively [14].

In corn breeding programs, beyond field-based plant phenotyping, accurately and efficiently phenotyping corn ears presents a significant challenge [15]. Traits directly associated with grain yield, such as ear length, width, number of rows, and number of grains per ear, are notoriously labor-intensive to measure, especially when evaluating numerous genotypes in selection processes [16]. Moreover, manual phenotyping is vulnerable to inaccuracies due to differences in evaluator qualifications, calibration issues with the equipment used, and evaluator fatigue, both physical and mental [17].

In response to the challenges of manual ear phenotyping, image analysis has emerged as a valuable solution. It offers a non-destructive, cost-effective, and efficient alternative, showing a strong correlation with manually obtained data. Several studies have highlighted the potential of automated ear phenotyping to enhance the accuracy and speed of field data processing, aiding breeders in identifying desirable traits for the selection of superior genotypes. This technology is making significant strides in extracting information from cereal crops, including corn [18–25]. While some methods require rotating mechanisms to capture images of the entire ear surface, which increases both cost and time, others utilize a simpler approach by acquiring a single image of the ear [25–28].

Therefore, this study aims to estimate the correlation between vegetation indices (VIs) and grain yield and to identify the optimal timing and VIs for accurately estimating corn grain yield. Additionally, this study intends to utilize photographic quantification to measure the characteristics of corn ears and to establish their correlation with corn grain yield.

2. Materials and Methods

2.1. Study Area

The experiments were conducted in three different environments within the southern region of the state of Minas Gerais, Brazil, as illustrated in Figure 1. The first experimental site was located at the Center for Scientific and Technological Development of Agriculture (Fazenda Muquém) at the Federal University of Lavras (UFLA). This site is situated in the municipality of Lavras at an altitude of 954 m, with a latitude of 21°12'11" S and

longitude of 44°58'47" W. The second experimental location was the Agricultural Scientific and Technological Development Center—Fazenda Palmital, located in the municipality of Ijaci. It lies at a latitude of 21°09' S, a longitude of 44°54' W, and an altitude of 920 m. The third site was the experimental area of Science, Technology, and Engineering at Rehagro Pesquisa, located in the municipality of Nazareno at a latitude of 21°15'32" S, a longitude of 44°30'56" W, and an altitude of 1003 m.

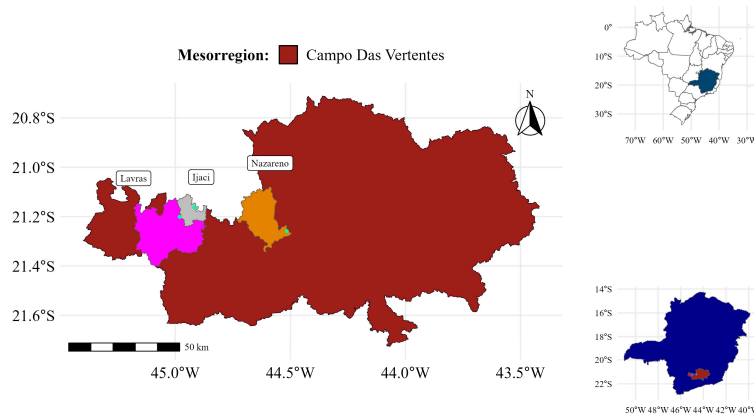


Figure 1. Map of experimental locations, in the cities of Lavras (pink color), Ijaci (gray color), and Nazareno (orange color) in the municipality of Minas Gerais (blue color) in Brazil.

2.2. Environmental Conditions

Climatic data were collected at each experimental location, as shown in Figure 2 [29], to monitor environmental conditions and inform decision-making regarding management practices in the experiments. These practices included determining the optimal sowing time, scheduling pesticide applications, planning data collection, and timing the harvest.

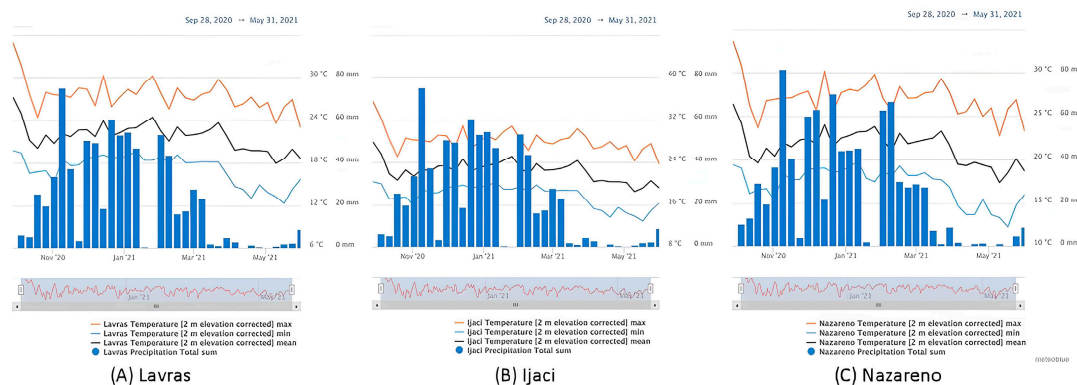


Figure 2. Climatic conditions of temperature and precipitation in the experimental areas of Lavras (A), Ijaci (B), and Nazareno (C) in the state of Minas Gerais in Brazil.

2.3. Experimental Management

Prior to sowing in the experimental areas, the production system was carefully prepared. This preparation involved implementing crop rotation, incorporating straw into the system, and utilizing machinery that minimized soil disturbance [30]. Sowing took place in the first half of November, with two seeds sown per hole. Subsequently, the experimental plots were thinned to ensure optimal plant density. Corrective fertilization for the experiments was conducted in line with the recommendations provided in [31], considering the unique soil characteristics and requirements of each location. Management of pests, diseases, and weeds was executed following the established guidelines for corn cultivation, tailored to the production goals and conditions of each experimental area [32].

2.4. Experimental Scheme

The experimental plots were laid out in a randomized block design, with each plot consisting of two rows that were five meters in length and spaced 0.60 m apart. Each treatment was replicated three times across the blocks. The corn hybrids evaluated in this study originated from four distinct heterotic groups, which were developed through the Recurrent Reciprocal Selection (RRS) program at the Federal University of Lavras (UFLA). These groups were designated as populations A, B, C, and D. Populations A and B consisted of conventional hybrids, whereas populations C and D featured hybrids with genetically modified traits, specifically Roundup Ready (RR) and *Bacillus thuringiensis* (BT) technology.

The experiments were conducted separately for the AB and CD populations. The AB experiment included a total of 10 treatments: six hybrids from the AB heterotic groups, the original populations A and B, and two commercial hybrids (Manufacturers Dekalb and KWS seeds, with the city and country of origin of the hybrids in the state of Minas Gerais in Brazil), DEKALB 230 PRO3 and RB 9077 PRO. The CD experiment followed the same procedure and featured the same commercial hybrids as checks.

2.5. Data Acquisition in the Field

Grain yield was assessed at the time of harvest. To standardize the yield data across all plots, the grain moisture content was corrected to 13%. The yield was subsequently calculated and is reported in kilograms per hectare ($\text{kg}\cdot\text{ha}^{-1}$).

Manual evaluations were conducted on three ears from each plot. A millimeter caliper was used to measure key characteristics related to grain yield, which included:

Length (L): the vertical distance from the base to the tip of the ear.

Width (W): the horizontal distance across the ear at its midpoint, between the rows of grains.

Total number of grains (TNG): the full count of grains on an ear.

2.6. Image Acquisition and Processing

To ensure the capture of high-quality images, a wooden box with overhead artificial lighting was used (as shown in Figure 3A). A contrasting background was also employed to enhance the distinction between the ears and their surroundings, thereby improving image quality. The captured ear images were then analyzed using the OpenCV and skimage libraries within the Python programming [33] environment to extract pertinent information (Figure 3B).

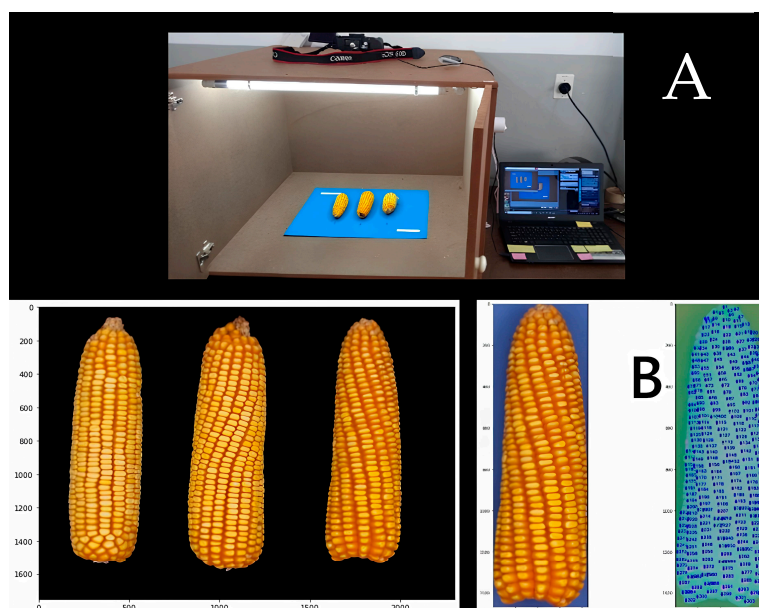


Figure 3. Chamber for image capture (A). Ears without the background and grain count (B).

For the correlation studies, RGB digital images of the ears were taken using a Canon EOS 60D professional-grade camera, which was equipped with a 35 mm lens. The lens featured a built-in autofocus motor and an aperture setting of f/1.8. To maintain consistency across all images, the camera’s ISO was set to a fixed value of 1200. The images were recorded in the ‘JPG’ format and utilized the RGB color system, comprising the red, green, and blue color channels.

In this study, a DJI Mavic Pro UAV (DJI Technology Co., Ltd, located in Shenzhen in China) was employed, which was equipped with a 1/2.3” CMOS RGB digital camera. The camera has an effective pixel count of 12.35 million (with a total of 12.71 million pixels). UAV flights were conducted under optimal weather conditions, featuring clear skies and minimal wind, and were scheduled between 10:00 and 14:00 local time to ensure consistent lighting. The UAV was flown at an altitude of 30 m above the crop plots to capture aerial imagery (Figure 4).

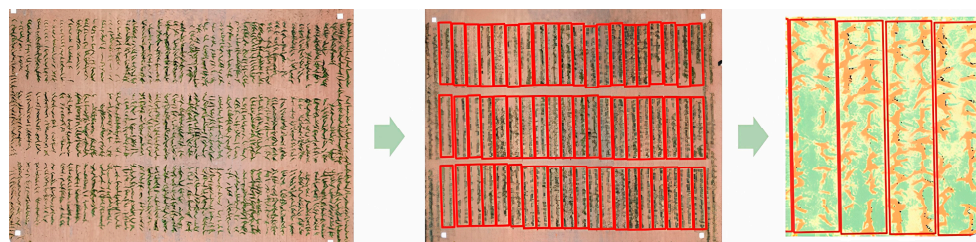


Figure 4. Images captured using a UAV equipped with an RGB camera, flying at a height of 30 m above the plots, with the resulting segments from an orthomosaic.

Flight paths were meticulously planned using the Pix4D (PIX4D S.A., Renens in Switzerland) [34] Capture app to achieve 80% longitudinal and 60% lateral overlap, ensuring thorough coverage of the plots. Orthomosaics were generated from the collected images using the Agisoft PhotoScan Professional software (Agisoft LLC, located in St. Petersburg in Russia; version 1.8.5 BUILB 15259) [35]. For the analysis of the aerial data and evaluation of crop growth, the R programming [36] environment was utilized, along with the FIELDimageR package, which is specifically designed for agricultural image analysis.

In the evaluation and monitoring of crop growth, various vegetation indices were computed. These indices involve algebraic operations on values derived from distinct spectral bands in the visible spectrum. Notably, the indices include the Normalized Green-Red Difference Index (NGRDI), Visible Atmospherically Resistant Index (VARI), Green Leaf Index (GLI), and Excess Green Color Index (ExG) (Table 1) [37–40]. Subsequently, these indices enable correlation with various crop variables, such as biomass, canopy cover, chlorophyll content, and grain yield [41,42]. This paper focuses on the correlation with grain yield.

Table 1. Description index formulas and equations.

Index	Equations	References
NGRDI	$(G - R)/(G + R)$ (1)	[37]
VARI	$(G - R)/(G + R - B)$ (2)	[38]
GLI	$(2 * G - R - B)/(2 * G + R + B)$ (3)	[39]
ExG COLOR INDEX	$2 * g - r - b$ (4)	[40]

R = red, G = green, and B = blue.

$$r = \frac{R}{R + G + B} \tag{5}$$

$$g = \frac{G}{R + G + B} \tag{6}$$

$$b = \frac{B}{R + G + B} \tag{7}$$

The flights were performed at different vegetative and reproductive stages to capture the entire crop development cycle (Table 2).

Table 2. UAV flight and corn vegetative/reproductive stage in each location.

	Flight 1	Flight 2	Flight 3	Flight 4
Ijaci	V5	VT	R3	R5
Lavras	V5	V10	VT	R3
Nazareno	V8	VT	R4	R6

2.7. Pre-Processing of Data and Statistical Analysis

Individual analyses for all traits were carried out using the statistical model as follows (Equation (8)):

$$y_{ij} = \mu + h_i + b_j + e_{ij} \tag{8}$$

where:

y_{ij} : observed value for the plot that received hybrid i in block j .

μ : constant associated with every observation.

h_i : effect of hybrid i .

b_j : effect of block j .

e_{ij} : error associated with hybrid i in block j .

Furthermore, joint analyses for all traits were performed using the statistical model as follows (Equation (9)):

$$y_{ijk} = \mu + h_i + b_j(k) + l_k + h * lik + e_{ijk} \tag{9}$$

where:

y_{ijk} : observed value for the plot that received hybrid i in block j at location l .

μ : constant associated with every observation.

h_i : effect of hybrid i .

b_j : effect of block j in location k .

l_k : effect of location k .

$h * lik$: effect of hybrid-by-location interaction.

e_{ijk} : error associated with hybrid i in block j at location k .

Experimental precision plays a vital role in ensuring the quality and reliability of trials. Accurate experiments yield more dependable estimates, leading to more precise recommendations. The precision of an experiment is closely tied to its ability to reproduce results consistently. In this study, the Coefficient of Variation (CV) was employed to assess experimental precision. The CV considers both the residual variation and the experimental mean. The accuracy of the results depends on the magnitude of the residual variation, the number of replications, and the balance between genetic and residual variations associated with the specific trait being evaluated [43].

To assess experimental precision, the coefficient of variation and accuracy were estimated using Equation (10). Accuracy was determined using the following estimator:

$$\hat{r}_{gg} = \sqrt{1 - \left(\frac{1}{F}\right)} \tag{10}$$

where the F-value (from Snedecor) represents the variance ratio for the effects of treatments (hybrids) and is associated with the analysis of variance (ANOVA). The coefficient of variation was estimated using the following estimator, as shown in Equation (11):

$$CV = \frac{\sqrt{\sigma_E^2}}{\bar{x}} \quad (11)$$

where:

σ_E^2 : residual variation.

\bar{x} : hybrid means.

The analysis of the phenotypic Pearson correlation between field data (grain yield) and aerial images obtained via UAV was calculated. For digital ear images, the correlation between manual and photographic measurements for traits such as width, length, and total number of grains (TNG) was performed. To verify the efficiency of phenotyping through digital images and its agreement with manual phenotyping, some reliability measures described in the literature were estimated for these characteristics using the software GENES (version 1990.2023.15) [44] and R (version 4.1.3) [36].

The reliability measures used included the Coefficient of Determination (R^2) from simple linear regression without an intercept (model: $Y = \beta X + e$, where Y is the value obtained from the analysis of images, β is the angular coefficient, and X is the value obtained with manual measurement). Additionally, the Pearson (r) correlation was calculated (Equation (12)), according to the classification proposed by Hopkins (2000):

$$r = \frac{\sum_{i=1}^n (X_i - \bar{X}) * (Y_i - \bar{Y})}{\sqrt{\sum_{i=1}^n (X_i - \bar{X})^2} * \sqrt{\sum_{i=1}^n (Y_i - \bar{Y})^2}} \quad (12)$$

where X_i corresponds to the i -th value obtained with manual measurement, Y_i represents the i -th value observed from the image analysis, \bar{X} is the mean of the values obtained by manual measurement, and \bar{Y} is the mean of the values observed from the image analysis.

The Huber M-estimation method (Robust Fit) was used to test the regression (Equation (13)). Huber M-estimation finds parameter estimates that minimize the Huber loss function (Equation (14)):

$$l(e) = \sum_i p(e_i) \quad (13)$$

where:

$$p(e) = \begin{cases} \frac{1}{2}e^2 & \text{if } |e| < k \\ k|e| - \frac{1}{2}k^2 & \text{if } |e| \geq k \end{cases} \quad (14)$$

e refers to the residuals.

The Huber loss function penalizes outliers and increases quadratically for small errors and linearly for large errors [45,46].

3. Results and Discussion

An individual variance analysis revealed significant differences in grain yield among hybrids in both populations and across all three locations [47]. Experimental precision, assessed using the coefficient of variation (CV) and accuracy ($r\hat{g}g^2$), demonstrated high experimental precision with CVs consistently within the low to medium range. Accuracy was also consistently high, ranging from 79.07% to 95.94% across all trials.

A joint variance analysis indicated significant differences between genetic treatments, environments, and hybrid-by-environment interactions for grain yield [48]. Grain yield means varied from 6739 to 12,156 kg/ha for the AB population and from 6236 to 12,930 kg/ha for the CD population. The Scott-Knott test [49] categorized the hybrids into two distinct groups for both populations (Table 3). In the AB trials, hybrids RB 9077 and DKB 230 demonstrated the highest grain yield performance, while the lowest performance was observed in the remaining AB hybrids. For the CD population, hybrids RB 9077, DKB 230, and Hybrid CD1 exhibited the highest grain yield performance, along with other high-performing CD hybrids.

Table 3. Comparing the grain yield means (kg/ha) of the 10 AB and CD maize hybrids in three different environments using the Scott-Knott test.

Hybrids AB	AB Mean	Hybrids CD	CD Mean
RB 9077	12,156 a	RB 9077	12,930 a
DKB 230	10,623 a	DKB 230	11,151 a
Hybrid AB 2	9707 b	Hybrid CD 2	7445 b
Hybrid AB 1	9559 b	Hybrid CD 1	10,235 a
Hybrid AB 4	9468 b	Hybrid CD 4	8242 b
Hybrid AB 5	9466 b	Hybrid CD 5	8711 b
Hybrid AB 6	9363 b	Hybrid CD 6	6236 b
Hybrid AB 3	8868 b	Hybrid CD 3	8732 b
Hybrid AB	8306 b	Hybrid AB	10,108 a
Hybrid CD	6739 b	Hybrid CD	7525 b

Means followed by the same letter in the columns belong to the same group, according to Ref. [49], with to the level of a probability of 5%.

In the context of field phenotyping, the estimation of vegetation indices demonstrated good experimental precision, as indicated by high accuracy and a low coefficient of variation, although specific data are not presented here. The precision of these parameters reflects the quality of the trials at the time the images were captured [50]. Generally, higher precision leads to a stronger correlation between yield and the vegetation index, which was evident during flights 1, 2, and 3.

However, flight 4 at the Nazareno location, particularly when the trials were assessed towards the end of the crop cycles, exhibited lower precision. This reduction in precision was attributed to the emergence of weeds as the corn plants began to senesce [51]. Consequently, a negative correlation between vegetation indices and yield was observed, characterized by a negative regression slope. A similar impact of weed interference on such measurements has been reported in the literature [52].

In the combined analysis of all traits, both location and flight were determined to have a statistically significant impact. Consequently, separate regression analyses were performed for these variables. Flight 1, which coincided with the V5 growth stage for plants in Lavras and Ijaci and the V8 stage in Nazareno, demonstrated strong R-squared values in relation to grain yield for both populations across all vegetation indices (VIs) and green leaf areas. Similarly, during the VT growth stage, a good correlation between yield and VI was observed. Generally, the highest R-squared values were associated with the Green Leaf Index (GLI) and the Excess Green (ExG) indices, as indicated in Table 4. Figure 5 illustrates the regression slopes for each flight at the respective locations.

Table 4. R-squared coefficient between four vegetation indices and green leaf area with grain yield (YD) for each of the three locations and each flight.

	Flight 1					Flight 2				
	NGRDI	VARI	GLI	ExG	Area	NGRDI	VARI	GLI	ExG	Area
Lavras	0.07 *	0.05	0.09 *	0.09 *	0.02	0.09 *	0.09 *	0.07 *	0.07 *	0.09 **
Ijaci	0.03	0.01	0.19 **	0.19 **	0.01	0.14 *	0.14 **	0.08 *	0.06 *	0.15 **
Nazareno	0.04	0.03	0.02	0.04 *	0.11 **	0.07 *	0.06 *	0.07 *	0.07 *	0.09 **
	Flight 3					Flight 4				
	NGRDI	VARI	GLI	ExG	Area	NGRDI	VARI	GLI	ExG	Area
Lavras	0.08 **	0.10 **	0.03	0.03	0.05	0.003	0.004	0.001	0.001	0.0003
Ijaci	0.08 *	0.07 *	0.12 **	0.13 **	0.06	0.02	0.01	0.06 *	0.06 *	0.00
Nazareno	0.04	0.03	0.03	0.03	0.02	0.12 **	0.12 **	0.05	0.05	0.001

R-squared coefficient: ** ($p < 0.01$), * ($p < 0.05$), values without an asterisk sign represent nonsignificant correlations according to the Robust Fit test using the Huber M-estimation method.

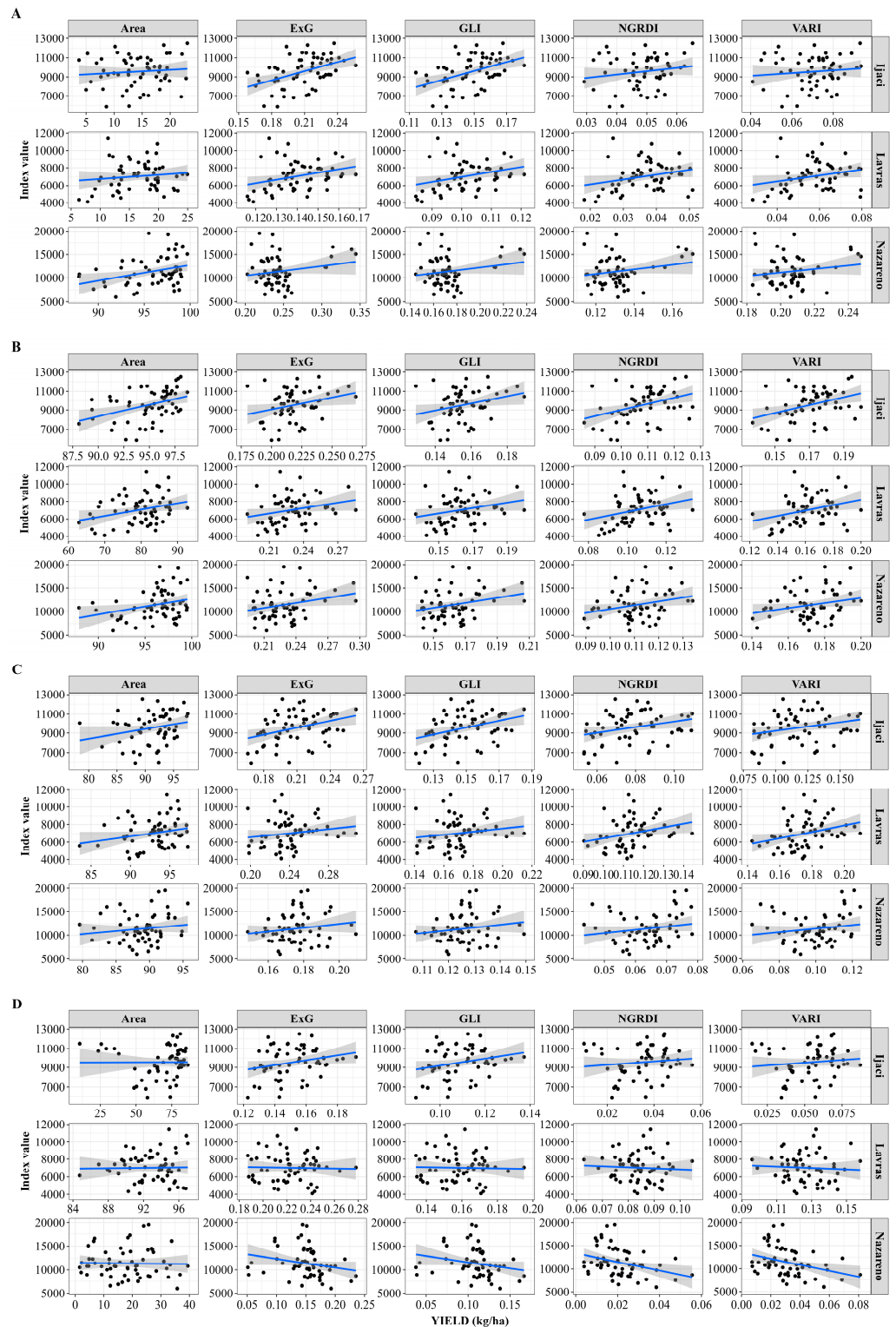


Figure 5. Dispersion graph of the vegetation index and area versus yield for the four flights and the three locations, with standard deviation represented in gray. (A) Flight 1, (B) Flight 2, (C) Flight 3, and (D) Flight 4.

Recent analyses of durum wheat in Spain have demonstrated that RGB picture vegetation indices consistently surpass multispectral indices like NDVI in both yield prediction and disease detection capabilities [53]. At the canopy level, RGB indices showed a strong correlation with grain yield (GY) and GY losses due to disease presence, with R^2 values of 0.581 and 0.536, respectively. In contrast, NDVI was significantly less accurate, with

R^2 values of only 0.261 and 0.277, respectively, particularly at later growth stages [54]. A similar trend has been noted in corn, where RGB vegetation indices derived from canopy images emerged as the best predictors of grain yield across different nitrogen fertilization treatments, achieving an R^2 of 0.721. These RGB indices outperformed both aerial and ground-based NDVI measurements, which had R^2 values of 0.689 and 0.293, respectively [54].

Some crops have exhibited a relatively high correlation between VI and yield. For instance, the NGRDI has been positively and significantly correlated with the aboveground biomass of peas and oats, with R^2 values ranging from 0.58 to 0.78 [13–55]. However, in corn, the correlation between VI and yield varied according to the growth stage and the specific index used. The Visible VARI and NGRDI showed correlations of 0.52 and 0.47, respectively [14–56]. These correlations were consistent with the findings of this study. Beyond VI, canopy cover has also been reported as a good predictor for corn yield. Specifically, canopy cover at 47 and 79 days after sowing demonstrated correlations with grain yield of 0.76 and 0.77, respectively [14]. According to [57], the most precise correlation between yield potential levels in maize and the NDVI index occurred at the V3 and V8 growth stages, with the highest correlation observed at V8. This pattern was also observed in the current study.

Corn yield is influenced by a multitude of environmental factors. Moreover, maize yield per unit area is not solely dependent on yield per plant but is also associated with a variety of traits. These include tolerance to biotic and abiotic stresses, adaptability to climatic and weather conditions, tolerance to planting density, and resistance to lodging. These traits add complexity and pose challenges for establishing direct correlations between yield and individual simple traits [58].

While plant area and VI are linked to yield for different maize varieties, the yield per plant is primarily determined by the yield per ear. This, in turn, is a function of grain number (GN) and grain weight (GW). GN can be further broken down into ear row number (ERN) and grain number per row (GNPR). By decomposing maize yield into its constituent components, researchers can facilitate more in-depth genetic and molecular studies aimed at understanding the determinants of maize yield [58].

In the process of corn ear phenotyping, a diverse set of 530 ears was analyzed, exhibiting substantial phenotypic variation across all assessed descriptors. This diversity was crucial for the validation of the proposed methodologies, as it included a wide range of ear patterns. The lengths of the ears ranged from 11.8 to 22.6 cm, while the widths spanned from 3.83 to 6.12 cm. The estimated regression coefficients (R^2) for ear width and ear length were notably high, at 0.92 (Figure 6A) and 0.88 (Figure 6B), respectively. These high R^2 values demonstrate a strong correlation between the measurements obtained through traditional manual phenotyping and those acquired via imaging techniques, underscoring the reliability of the latter in capturing ear dimensions.

Width measurements were conducted using a digital caliper, ensuring higher precision, while length measurements were taken with a ruler. The validity of these measurements is further supported by Pearson's correlation coefficient, which was calculated separately for different populations and locations (Table 5).

Generally, manual measurements demonstrated lower accuracy for all assessed traits compared to photographic measurements, as indicated by the accuracy values presented in Table 5 [59]. When examining the trials individually, width measurements showed the highest correlation, with all trials exhibiting correlations greater than 0.90 [60]. For length measurements, the correlations were also very high, although the lowest was 0.83, observed in the Lavras CD trial. The correlation for the total number of grains (TNG) varied, ranging from 0.65 in the Ijaci AB trial to 0.80 in the Lavras CD trial (Table 5). When aggregating all the data, the highest correlation was observed for width, with an R^2 of 0.91 (Figure 6A), followed by length, which had a robust R^2 of 0.87 (Figure 6B). This discrepancy may be attributable to the different measurement methods used; width was measured with a caliper, which typically offers greater precision, while length was measured with a ruler.

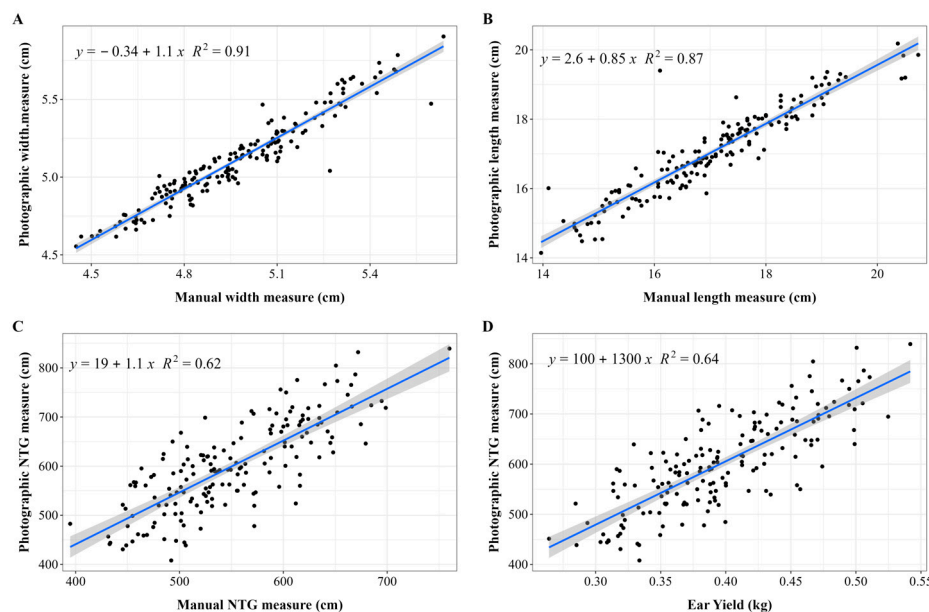


Figure 6. Dispersion graph from manual versus photographic measurements for the trait width (A), length (B), TNG (C), and corn ear yield with photographic TNG measurements (D) and multiple R-squared (R^2). Standard deviation in gray.

Table 5. Accuracy for manual and photographic width, length, TNG, and correlation between manual and photographic measurements in the AB and CD populations in Ijaci, Lavras and Nazareno.

	Manual Accuracy			Photographic Accuracy			Correlation		
	Width	Length	TNG	Width	Length	TNG	Width	Length	TNG
Ijaci AB	68.95	67.94	84.56	77.12	72.85	84.58	0.90 **	0.95 **	0.65 **
Ijaci CD	85.55	74.48	76.00	82.58	73.27	87.86	0.96 **	0.98 **	0.70 **
Lavras AB	65.99	72.54	65.26	81.96	75.20	83.31	0.95 **	0.95 **	0.79 **
Lavras CD	92.39	17.78	78.82	93.66	69.47	83.77	0.98 **	0.83 **	0.80 **
Nazareno AB	57.02	80.58	83.73	71.58	79.97	93.52	0.97 **	0.97 **	0.75 **
Nazareno CD	79.78	82.20	51.23	78.62	80.78	64.96	0.98 **	0.97 **	0.71 **

Pearson’s correlation coefficient: ** ($p < 0.01$), values without an asterisk sign represent nonsignificant correlations according to the *t*-test.

The R^2 value for the NTG between manual and photographic measurements was 0.62, as shown in Figure 6C. Additionally, the association between photographic measurements and ear yield was represented by an R^2 of 0.64 (Figure 6D). Phenotyping that utilizes imaging to estimate the number of grains offers significant advantages, such as automation, cost-effectiveness, improved accuracy, and reduced time and labor requirements. In contrast, manual measurements are highly subjective and can be influenced by human factors, as indicated by references [18–61].

The methodology presented for estimating length and width demonstrated remarkable consistency, suggesting that its integration into breeding programs could significantly enhance the efficiency of ear phenotyping. By adopting this approach, breeders can expect to see a reduction in the time required for data collection and a minimization of human errors, which are common with manual measurements. This improvement in phenotyping processes is crucial for the rapid selection and advancement of superior genotypes.

These findings are consistent with the existing literature, which indicates that high concordance indices, often approaching unity, have been observed in the estimation of leaf area using digital images. Such high levels of agreement suggest that digital image analysis can provide a reliable and robust alternative to traditional measurement techniques.

Previous studies have similarly concluded that image analysis can effectively replace manual phenotyping by providing more precise measurements of relevant descriptors [62]. This is particularly pertinent in the context of high-throughput phenotyping, where the ability to measure many plants quickly and accurately is essential.

In addition to improving accuracy and efficiency, the use of image-based phenotyping tools can also facilitate the collection of data that might be challenging to measure manually. For example, digital images of ears can be analyzed to capture subtle phenotypic variations that are critical in the seed industry for estimating yield loss during seed beneficiation. Moreover, the digital data obtained can be easily stored, shared, and reanalyzed, enhancing the reproducibility of research findings and facilitating collaborative breeding efforts.

The adoption of image-based phenotyping is also in line with the trend towards precision agriculture, where data-driven decision making is key to optimizing crop production. By leveraging advanced image analysis techniques, breeders and agronomists can gain deeper insights into plant traits, ultimately leading to the development of crop varieties that are better suited to meet the demands of a growing global population and changing climatic conditions.

4. Conclusions

The adoption of digital imaging has demonstrated considerable potential as a method for evaluating the components of corn production, and thus its yield. The most suitable phenological stages for data collection have been determined to be V5 and VT, with the least favorable observations noted at the R5 stage. Indices such as the Green Leaf Index (GLI) and the Excess Green (ExG) have demonstrated high values of correlation with corn production parameters. However, it is crucial to acknowledge the substantial variability in vegetation index values according to environmental conditions and phenological stages.

The compatibility of digital image analysis with traditional manual measurements has been demonstrated as a practical tool, with a strong correlation observed for parameters such as ear width and length.

Given these findings, the continuation and expansion of research in this area are highly recommended. By doing so, more precise decision making can be facilitated, potentially leading to substantial improvements in corn production.

Author Contributions: E.L.R.: conceptualization, formal analysis, investigation, methodology, and writing—original draft; A.T.B.: formal analysis, investigation, methodology, supervision, and writing—original draft. E.d.S.C.: formal analysis, investigation, and methodology. V.Q.C.: investigation and methodology. V.A.P.d.S.: investigation and writing—original draft. P.H.F.C.B.: writing—original draft and writing—review and editing. R.R.P.: investigation. All authors have read and agreed to the published version of the manuscript.

Funding: This research received funding from Capes (for the PhD scholarship) and CNPq (for the grant productivity fellow).

Data Availability Statement: Data are contained within this article.

Acknowledgments: The authors thank the Federal University of Lavras for the structure and the funding bodies.

Conflicts of Interest: The authors declare no conflicts of interest.

References

1. Dos Santos, C.V.; de Moraes, F.A.; Torres, L.G.; da Silva, R.A.; da Silva, K.J.; Moreira, S.G.; de Menezes, C.B.; Borém, A. Fenotipagem de raízes de milho visando tolerância à seca: Uma revisão. *Res. Soc. Dev.* **2021**, *10*, e24119817265. [[CrossRef](#)]
2. Moreira, F.F.; Oliveira, H.R.; Volenec, J.J.; Rainey, K.M.; Brito, L.F. Integrating high-throughput phenotyping and statistical genomic methods to genetically improve longitudinal traits in crops. *Front. Plant Sci.* **2020**, *11*, 681. [[CrossRef](#)] [[PubMed](#)]
3. Su, Y.; Wu, F.; Ao, Z.; Jin, S.; Qin, F.; Liu, B.; Pang, S.; Liu, L.; Guo, Q. Evaluating Maize Phenotype Dynamics under Drought Stress Using Terrestrial Lidar. *Plant Methods* **2019**, *15*, 11. [[CrossRef](#)] [[PubMed](#)]
4. Li, Y.; Wen, W.; Guo, X.; Yu, Z.; Gu, S.; Yan, H.; Zhao, C. High-Throughput Phenotyping Analysis of Maize at the Seedling Stage Using End-to-End Segmentation Network. *PLoS ONE* **2021**, *16*, e0241528. [[CrossRef](#)] [[PubMed](#)]

5. Bazakos, C.; Hanemian, M.; Trontin, C.; Jiménez-Gómez, J.M.; Loudet, O. New Strategies and Tools in Quantitative Genetics: How to Go from the Phenotype to the Genotype. *Annu. Rev. Plant Biol.* **2017**, *68*, 435–455. [[CrossRef](#)] [[PubMed](#)]
6. Song, P.; Wang, J.; Guo, X.; Yang, W.; Zhao, C. High-Throughput Phenotyping: Breaking through the Bottleneck in Future Crop Breeding. *Crop J.* **2021**, *9*, 633–645. [[CrossRef](#)]
7. Zhou, X.; Zheng, H.B.; Xu, X.Q.; He, J.Y.; Ge, X.K.; Yao, X.; Cheng, T.; Zhu, Y.; Cao, W.X.; Tian, Y.C. Predicting Grain Yield in Rice Using Multi-Temporal Vegetation Indices from UAV-Based Multispectral and Digital Imagery. *ISPRS J. Photogramm. Remote Sens.* **2017**, *130*, 246–255. [[CrossRef](#)]
8. Di Gennaro, S.F.; Rizza, F.; Badeck, F.W.; Berton, A.; Delbono, S.; Gioli, B.; Toscano, P.; Zaldei, A.; Matese, A. UAV-Based High-Throughput Phenotyping to Discriminate Barley Vigour with Visible and near-Infrared Vegetation Indices. *Int. J. Remote Sens.* **2018**, *39*, 5330–5344. [[CrossRef](#)]
9. Tewes, A.; Schellberg, J. Towards Remote Estimation of Radiation Use Efficiency in Maize Using UAV-Based Low-Cost Camera Imagery. *Agronomy* **2018**, *8*, 16. [[CrossRef](#)]
10. Li, B.; Xu, X.; Han, J.; Zhang, L.; Bian, C.; Jin, L.; Liu, J. The Estimation of Crop Emergence in Potatoes by UAV RGB Imagery. *Plant Methods* **2019**, *15*, 15. [[CrossRef](#)]
11. Lu, N.; Zhou, J.; Han, Z.; Li, D.; Cao, Q.; Yao, X.; Tian, Y.; Zhu, Y.; Cao, W.; Cheng, T. Improved Estimation of Aboveground Biomass in Wheat from RGB Imagery and Point Cloud Data Acquired with a Low-Cost Unmanned Aerial Vehicle System. *Plant Methods* **2019**, *15*, 17. [[CrossRef](#)] [[PubMed](#)]
12. Maimaitijiang, M.; Sagan, V.; Sidike, P.; Hartling, S.; Esposito, F.; Fritschi, F.B. Soybean Yield Prediction from UAV Using Multimodal Data Fusion and Deep Learning. *Remote Sens. Environ.* **2020**, *237*, 111599. [[CrossRef](#)]
13. Jannoura, R.; Brinkmann, K.; Uteau, D.; Bruns, C.; Joergensen, R.G. Monitoring of Crop Biomass Using True Colour Aerial Photographs Taken from a Remote Controlled Hexacopter. *Biosyst. Eng.* **2015**, *129*, 341–351. [[CrossRef](#)]
14. García-Martínez, H.; Flores-Magdaleno, H.; Ascencio-Hernández, R.; Khalil-Gardezi, A.; Tijerina-Chávez, L.; Mancilla-Villa, O.R.; Vázquez-Peña, M.A. Corn Grain Yield Estimation from Vegetation Indices, Canopy Cover, Plant Density, and a Neural Network Using Multispectral and RGB Images Acquired with Unmanned Aerial Vehicles. *Agriculture* **2020**, *10*, 277. [[CrossRef](#)]
15. Araus, J.L.; Kefauver, S.C.; Zaman-Allah, M.; Olsen, M.S.; Cairns, J.E. Translating High-Throughput Phenotyping into Genetic Gain. *Trends Plant Sci.* **2018**, *23*, 451–466. [[CrossRef](#)]
16. Yang, W.; Zhang, X.; Duan, L. High-Throughput Phenotyping (HTP) and Genetic Analysis Technologies Reveal the Genetic Architecture of Grain Crops. In *High-Throughput Crop Phenotyping*; Springer: Berlin/Heidelberg, Germany, 2021; pp. 101–127. [[CrossRef](#)]
17. Duddu, H.S.N.; Johnson, E.N.; Willenborg, C.J.; Shirliffe, S.J. High-Throughput UAV Image-Based Method Is More Precise than Manual Rating of Herbicide Tolerance. *Plant Phenom.* **2019**, *2019*, 6036453. [[CrossRef](#)]
18. Liang, X.; Wang, K.; Huang, C.; Zhang, X.; Yan, J.; Yang, W. A High-Throughput Maize Kernel Traits Scorer Based on Line-Scan Imaging. *Measurement* **2016**, *90*, 453–460. [[CrossRef](#)]
19. Miller, N.D.; Haase, N.J.; Lee, J.; Kaeppler, S.M.; de Leon, N.; Spalding, E.P. A Robust, High-throughput Method for Computing Maize Ear, Cob, and Kernel Attributes Automatically from Images. *Plant J.* **2017**, *89*, 169–178. [[CrossRef](#)]
20. Makanza, R.; Zaman-Allah, M.; Cairns, J.E.; Eyre, J.; Burgueño, J.; Pacheco, Á.; Diepenbrock, C.; Magorokosho, C.; Tarekge, A.; Olsen, M.; et al. High-Throughput Method for Ear Phenotyping and Kernel Weight Estimation in Maize Using Ear Digital Imaging. *Plant Methods* **2018**, *14*, 49. [[CrossRef](#)]
21. Chipindu, L.; Mupangwa, W.; Mtsilizah, J.; Nyagumbo, I.; Zaman-Allah, M. Maize Kernel Abortion Recognition and Classification Using Binary Classification Machine Learning Algorithms and Deep Convolutional Neural Networks. *AI* **2020**, *1*, 361–375. [[CrossRef](#)]
22. Matias, F.I.; Caraza-Harter, M.V.; Endelman, J.B. FIELDImageR: An R Package to Analyze Orthomosaic Images from Agricultural Field Trials. *Plant Phenome J.* **2020**, *3*, e20005. [[CrossRef](#)]
23. Wu, D.; Cai, Z.; Han, J.; Qin, H. Automatic Kernel Counting on Maize Ear Using RGB Images. *Plant Methods* **2020**, *16*, 79. [[CrossRef](#)]
24. Kienbaum, L.; Correa Abondano, M.; Blas, R.; Schmid, K. DeepCob: Precise and High-Throughput Analysis of Maize Cob Geometry Using Deep Learning with an Application in Genebank Phenomics. *Plant Methods* **2021**, *17*, 91. [[CrossRef](#)] [[PubMed](#)]
25. Warman, C.; Sullivan, C.M.; Preece, J.; Buchanan, M.E.; Vejlupekova, Z.; Jaiswal, P.; Fowler, J.E. A Cost-effective Maize Ear Phenotyping Platform Enables Rapid Categorization and Quantification of Kernels. *Plant J.* **2021**, *106*, 566–579. [[CrossRef](#)] [[PubMed](#)]
26. Darrah, L.L.; McMullen, M.D.; Zuber, M.S. Breeding, genetics and seed corn production. In *Em Corn*; Elsevier: Amsterdam, The Netherlands, 2019; pp. 19–41. ISBN 9780128119716.
27. Rebetzke, G.J.; Jimenez-Berni, J.; Fischer, R.A.; Deery, D.M.; Smith, D.J. Review: High-Throughput Phenotyping to Enhance the Use of Crop Genetic Resources. *Plant Sci.* **2019**, *282*, 40–48. [[CrossRef](#)] [[PubMed](#)]
28. Zhang, X.; Liu, J.; Song, H. Corn Ear Test Using SIFT-Based Panoramic Photography and Machine Vision Technology. *Artif. Intell. Agric.* **2020**, *4*, 162–171. [[CrossRef](#)]
29. Dados Históricos Simulados de Clima e Tempo Para Lavras. Available online: https://www.meteoblue.com/pt/tempo/historyclimate/climatemodelled/lavras_brasil_3458696 (accessed on 29 January 2024).

30. Salomão, P.E.A.; Kriebel, W.; dos Santos, A.A.; Martins, A.C.E. A importância do sistema de plantio direto na palha para reestruturação do solo e restauração da matéria orgânica. *Res. Soc. Dev.* **2020**, *9*, e154911870. [[CrossRef](#)]
31. Lorenzi, J.O.; Monteiro, P.A.; Miranda Filho, H.S.; Raij, B. *Recomendações de Adubação e Calagem para o Estado de São Paulo*; IAC: Campinas, Brazil, 1997; Volume 100, pp. 221–229.
32. Resende, E.L.; Pinho, R.G.V.; Silva, E.V.V.; Massitela, J.J.; de Souza, V.F.; Souza, J.L.D. Mean components for choosing maize populations to extract inbred lines. *Ciênc. Agrotecnologia* **2020**, *44*, e017820. [[CrossRef](#)]
33. Available online: <https://www.python.org/success-stories/category/scientific/> (accessed on 30 January 2024).
34. Professional Photogrammetry and Drone Mapping Software. Available online: <https://www.pix4d.com/> (accessed on 30 January 2024).
35. Agisoft Metashape: Agisoft Metashape. Available online: <https://www.agisoft.com/> (accessed on 30 January 2024).
36. The R Project for Statistical Computing. Available online: <https://www.r-project.org/> (accessed on 30 January 2024).
37. Tucker, C.J. Red and Photographic Infrared Linear Combinations for Monitoring Vegetation. *Remote Sens. Environ.* **1979**, *8*, 127–150. [[CrossRef](#)]
38. Gitelson, A.A.; Kaufman, Y.J.; Stark, R.; Rundquist, D. Novel Algorithms for Remote Estimation of Vegetation Fraction. *Remote Sens. Environ.* **2002**, *80*, 76–87. [[CrossRef](#)]
39. Louhaichi, M.; Borman, M.M.; Johnson, D.E. Spatially Located Platform and Aerial Photography for Documentation of Grazing Impacts on Wheat. *Geocarto Int.* **2001**, *16*, 65–70. [[CrossRef](#)]
40. Meyer, G.E.; Neto, J.C. Verification of Color Vegetation Indices for Automated Crop Imaging Applications. *Comput. Electron. Agric.* **2008**, *63*, 282–293. [[CrossRef](#)]
41. Sakamoto, T.; Gitelson, A.A.; Nguy-Robertson, A.L.; Arkebauer, T.J.; Wardlow, B.D.; Suyker, A.E.; Verma, S.B.; Shibayama, M. An Alternative Method Using Digital Cameras for Continuous Monitoring of Crop Status. *Agric. For. Meteorol.* **2012**, 154–155, 113–126. [[CrossRef](#)]
42. Maimaitijiang, M.; Ghulam, A.; Paheding, S.; Hartling, S. Unmanned aerial system (UAS)—Based phe-notyping of soybean using multi-sensor data fusion and extreme learning machine. *ISPRS J. Photogramm. Remote Sens.* **2017**, *134*, 43–58. [[CrossRef](#)]
43. De Resende, M.D.V.; Duarte, J.B. Precisão e controle de qualidade em experimentos de avaliação de cultivares. *Pesqui. Agropecuária Trop.* **2007**, *37*, 182–194.
44. Cruz, C.D. GENES—A software package for analysis in experimental statistics and quantitative genetics. *Acta Sci. Agron.* **2013**, *35*, 271–276. [[CrossRef](#)]
45. Huber, P.J. Robust Regression: Asymptotics, Conjectures and Monte Carlo. *Ann. Stat.* **1973**, *1*, 799–821. [[CrossRef](#)]
46. Ronchetti, E.M.; Huber, P.J. *Robust Statistics*; John Wiley & Sons: Hoboken, NJ, USA, 2009.
47. Rodene, E.; Xu, G.; Palali Delen, S.; Zhao, X.; Smith, C.; Ge, Y.; Schnable, J.; Yang, J. A UAV-based High-throughput Phenotyping Approach to Assess Time-series Nitrogen Responses and Identify Trait-associated Genetic Components in Maize. *Plant Phenome J.* **2022**, *5*, e20030. [[CrossRef](#)]
48. Cooper, M. Integração de ganho genético e análise de lacunas para prever melhorias na produtividade das culturas. *Crop Sci.* **2020**, *60*, 582–604. [[CrossRef](#)]
49. Scott, A.J.; Knott, M. A cluster analysis method for grouping means in the analysis of variance. *Biometrics* **1974**, *30*, 507. [[CrossRef](#)]
50. Chivasa, W.; Onísimo; Burgueno, J. Fenotipagem de alto rendimento baseada em UAV para aumentar a precisão da previsão e seleção em variedades de milho sob inoculação artificial de MSV. *Comput. E Eletrônica Na Agric.* **2021**, *184*, 106128. [[CrossRef](#)]
51. Galon, L. Períodos de interferência de plantas daninhas infestando a cultura do milho. *Rev. De Ciências Agrárias* **2018**, *17*, 197–205.
52. Yu, N.; Li, L.; Schmitz, N.; Tian, L.F.; Greenberg, J.A.; Diers, B.W. Development of Methods to Improve Soybean Yield Estimation and Predict Plant Maturity with an Unmanned Aerial Vehicle Based Platform. *Remote Sens. Environ.* **2016**, *187*, 91–101. [[CrossRef](#)]
53. Khan, Z.; Rahimi-Eichi, V.; Haefele, S.; Garnett, T.; Miklavcic, S.J. Estimation of vegetation indices for high-throughput phenotyping of wheat using aerial imaging. *Métodos Veg.* **2018**, *14*, 1–11. [[CrossRef](#)]
54. Kefauver, S.C.; El-Haddad, G.; Vergara-Diaz, O.; Araus, J.L. RGB picture vegetation indexes for High-Throughput Phenotyping Platforms (HTPPs). In *Remote Sensing for Agriculture, Ecosystems, and Hydrology XVII*; SPIE: St Bellingham, WA, USA, 2015; pp. 82–90.
55. Lussem, U. Avaliação de índices de vegetação baseados em RGB a partir de imagens de UAV para estimar a produção de forragem em pastagens. Os Arquivos Internacionais de Fotogrametria. *Sensoriamento Remoto E Ciências Da Informação Espac.* **2018**, *42*, 1215–1219.
56. Macedo, F. Estimativa da Produtividade e Biomassa Aérea do Milho (*Zea mays*) através de Índices de Vegetação na Ilha da Madeira. *Agricultura* **2023**, *13*, 1115.
57. Vian, A.L.; Bredemeier, C.; Silva, P.R.F.D.A.; Santi, A.L.; Silva, C.P.G.D.A.; Santos, F.L.D.O.S. Limites críticos de ndvi para estimativa do potencial produtivo do milho. *Rev. Bras. Milho Sorgo* **2018**, *17*, 91. [[CrossRef](#)]
58. Zhang, H.; Lu, Y.; Ma, Y.; Fu, J.; Wang, G. Genetic and Molecular Control of Grain Yield in Maize. *Mol. Breed.* **2021**, *41*, 18. [[CrossRef](#)]
59. Medeiros, A.D.; Pereira, M.D.; Silva, J.A. Processamento digital de imagens na determinação do vigor de sementes de milho. *Rev. Bras. Cienc. Agrar./Braz. J. Agric. Sci.* **2018**, *13*, 1–7. [[CrossRef](#)]
60. Ma, X.; Zhu, K.; Guan, H.; Feng, J.; Yu, S.; Liu, G. High-throughput phenotyping analysis of potted soybean plants using colorized depth images based on a proximal platform. *Remote Sens.* **2019**, *11*, 1085. [[CrossRef](#)]

61. Komyshev, E.; Genaev, M.; Afonnikov, D. Evaluation of the SeedCounter, A mobile application for grain phenotyping. *Front. Plant Sci.* **2017**, *7*, 1990. [[CrossRef](#)] [[PubMed](#)]
62. Ramos, F. Leaf blade area of different plants estimated by linear and dry matter measures, calibrated with the ImageJ software. *Interciencia* **2015**, *40*, 570–575.

Disclaimer/Publisher's Note: The statements, opinions and data contained in all publications are solely those of the individual author(s) and contributor(s) and not of MDPI and/or the editor(s). MDPI and/or the editor(s) disclaim responsibility for any injury to people or property resulting from any ideas, methods, instructions or products referred to in the content.